

Electronic structure and resonant inelastic x-ray scattering in Ta₂NiSe₅

D.A. Kukusta,¹ L.V. Bekenov,¹ A.N. Yaresko,² K. Ishii,³ T. Takayama,² H. Takagi,² and V.N. Antonov^{1,2}

¹*G. V. Kurdyumov Institute for Metal Physics of the N.A.S. of Ukraine,
36 Academician Vernadsky Boulevard, UA-03142 Kyiv, Ukraine*

²*Max-Planck-Institute for Solid State Research, Heisenbergstrasse 1, 70569 Stuttgart, Germany*

³*Synchrotron Radiation Research Center, National Institutes for
Quantum Science and Technology, Sayo, Hyogo 679-5148, Japan*

(Dated: July 31, 2024)

We study the electronic structure of Ta₂NiSe₅ in its low-temperature semiconducting phase, using resonant inelastic x-ray scattering (RIXS) at the Ta L_3 edge. We also investigate the electronic properties of Ta₂NiSe₅ within the density-functional theory (DFT) using the generalized gradient approximation in the framework of the fully relativistic spin-polarized Dirac linear muffin-tin orbital band-structure method. While ARPES, dc transport, and optical measurements indicate that Ta₂NiSe₅ is a small band-gap semiconductor, DFT gives a metallic nonmagnetic solution in Ta₂NiSe₅. To obtain the semiconducting ground state in Ta₂NiSe₅ we use a self-interaction correction (SIC) procedure by introducing an orbital-dependent potential V_l into the Hamiltonian. We investigate theoretically the x-ray absorption spectroscopy (XAS) and RIXS spectra at the Ni and Ta L_3 edges and analyze the spectra in terms of interband transitions. We investigate the RIXS spectra as a function of momentum transfer vector \mathbf{Q} and incident photon energy. Because Ta₂NiSe₅ possesses only fully occupied (Ni $3d$ and Se $4p$) and completely empty (Ta $5d$) shells with the formal valencies Ta⁵⁺ ($5d^0$), Ni⁰ ($3d^{10}$), and Se²⁻ ($4p^6$), both the Ni and Ta L_3 RIXS spectra belong to a charge transfer type with ligand-to-metal excitations.

PACS numbers: 75.50.Cc, 71.20.Lp, 71.15.Rf

I. INTRODUCTION

Transition-metal compounds containing $5d$ elements usually have a rich variety of novel electronic states emerged from competing interactions, including the on-site Coulomb repulsion U , crystal-electric field (CEF), and spin-orbit coupling (SOC). These compounds possess the on-site Coulomb repulsion and SOC of the same order of magnitude ($U \sim 1-2$ eV, $\lambda_{SOC} \sim 0.5$ eV) [1]. It can give rise to some fascinating phenomena, such as topological insulators [2–5], Mott insulators [6–10], Weyl semimetals [11–13], and quantum spin liquids [8, 14].

In this paper, we consider the transition-metal chalcogenide Ta₂NiSe₅, which has been studied recently in the respect of the possible realization of the excitonic insulator (EI) state [15–17]. This chalcogenide form a quasi-one-dimensional (1D) chain structure with Ni single and Ta double chains running along the a axis. Along the b axis the layers are loosely held together by van der Waals' forces [18]. High temperature measurements of resistivity have shown that Ta₂NiSe₅ is a small band gap semiconductor with quasi-1D anisotropic electron conduction [19]. The nature of the electronic structure of the Ta₂NiSe₅ orthorhombic phase (space group $Cmcm$) is still strongly debated and this phase is argued to be a semimetal [20–22], almost zero energy gap semiconductor with the energy gap $\Delta E \leq 0.05$ eV [23], or conventional semiconductor [16, 24, 25]. At critical temperature $T_c = 328$ K, however, an anomaly in the resistivity occurs, which was associated with the second-order structural phase transition from an orthorhombic to monoclinic phase [17, 19]. The resistivity exhibits insulating

behavior both above and below the transition temperature T_c [24]. The magnetic susceptibility exhibits diamagnetism in a wide temperature range (4.2–900 K) and shows a sudden drop (being more negative) $\leq T_c$ [19]. The characteristic energy gap according to optical conductivity and RIXS measurements reaches $\Delta E \sim 0.16$ eV $\leq T_c$ [23, 26, 27]. Tunneling spectroscopy estimates the energy gap ~ 0.3 eV at 78 K [22]. ARPES experiments showed that the spectra are strongly temperature dependent [15, 16]. At 40 K the valence band top flattens, the quasiparticle peak sharpens and the size of the band gap becomes larger. It was suggested that the EI state is realized as the ground state of this material, with excitons formed by a charge transfer between the Ni and Ta chains [15, 24, 28]. However, direct evidence of excitons and their behavior across the EI transition has thus far not been reported.

While ARPES, dc transport, and optical measurements indicate that Ta₂NiSe₅ is a small band-gap semiconductor, density functional theory (DFT) gives a metallic nonmagnetic solution in Ta₂NiSe₅ [17, 26]. The top of the valence band, formed by (almost) completely occupied Se $4p$ and Ni $3d$ states, overlaps with the bottom of the conduction band, which is derived from Ta $5d$ t_{2g} states hybridized with the chalcogen $4p$ ones. Thus, according to the DFT calculations the formal valencies are close to Ta⁵⁺ ($5d^0$), Ni⁰ ($3d^{10}$), and Se²⁻ ($4p^6$). Because Ta₂NiSe₅ possesses only fully occupied (Ni $3d$ and Se $4p$) and completely empty (Ta $5d$) shells it cannot be the subject for the application of the LDA+ U method. This method is not able to open up a gap [22, 26]. To reproduce the experimental band gap Kaneko *et al.* [17] introduce a self-interaction-like correction (SIC) proce-

ture [29, 30], where the conduction (valence) bands are shifted upward (downwards) by adding a SIC-like orbital-dependent potential V_l to the Hamiltonian so as to open up the gap in the band dispersion. The authors add the potentials $+V_l$ to the energy of the $5d$ orbitals of Ta and $-V_l$ to the energy of the $3d$ orbitals of Ni and $4p$ orbitals of Se in the orthorhombic structure. They found that the band gap actually opens up for $V_l = 4.2$ eV. They used the value of $V_l = 5.0$ eV in their band structure calculations. A similar procedure was used also in Ref. [26] to calculate the electronic structure and optical spectra in monoclinic Ta_2NiSe_5 . They found that the best agreement between the theoretically calculated and experimentally measured optical spectra is obtained when applying the orbital-dependent potential V_l only to the Se $4p$ states ($V_{Se4p} = -2.5$ eV).

In the present study, we focus on the electronic structure and resonant inelastic x-ray spectra (RIXS) of Ta_2NiSe_5 . RIXS measurements have been successfully performed at the Ni L_3 edge for Ta_2NiSe_5 by Monney *et al.* [31]. The authors present a RIXS map as a function of the incident photon energy, measured at the Ni L_3 edge as well as the in-plane momentum Q_x dispersion with σ -polarized incident light at 30 K. They also present the x-ray absorption spectroscopy (XAS) spectrum measured at the Ni L_3 edge by the total fluorescence yield. They obtained a band gap at the center of the Brillouin zone of ~ 0.35 eV at $\leq T_c$. The authors also estimated the effective valence m_V and conductive m_C band masses in close vicinity to the Fermi level. These masses were found to be rather large: $m_V = 0.8m_e$ and $m_C \sim 0.9\div 1.3m_e$. Lu *et al.* also measured the RIXS spectra at the Ta and Ni L_3 edges in a small energy interval up to 1.2 eV [27]. Below T_c , their RIXS energy-momentum map shows a band gap at the Brillouin zone center of ~ 0.16 eV. The authors interpreted the RIXS spectra in terms of the momentum-resolved joint density of states (JDOS) without taking into account corresponding matrix elements.

Although there has been great progress in the RIXS experiments over the past decade, the number of theoretical calculations of RIXS spectra is extremely limited. The most calculations of the RIXS spectra of various materials have been carried out using the atomic multiplet approach with several adjustable parameters. The question is to what extent DFT is able to reveal the aspects of RIXS spectra. In this paper, we report the experimentally measured RIXS spectrum of Ta_2NiSe_5 at the Ta L_3 edge in a wide energy interval as well as a detailed theoretical investigation of the electronic structure and RIXS spectra at the Ta and Ni L_3 edges. The energy band structure of this transition metal chalcogenide was calculated using the fully relativistic spin-polarized Dirac linear muffin-tin orbital band-structure method.

The paper is organized as follows. The crystal structure of Ta_2NiSe_5 and computational details are presented in Sec. II. Section III presents the electronic structure of the chalcogenide. In Sec. IV theoretical investigations of the RIXS spectra of Ta_2NiSe_5 at the Ni and Ta L_3 edges

are presented, and the theoretical results are compared with experimental measurements. Here, we also report the results of the calculations of x-ray absorption spectra at the Ni and Ta L_3 edges. Finally, the results are summarized in Sec. V.

II. EXPERIMENTAL AND COMPUTATIONAL DETAILS

A. X-ray magnetic circular dichroism

Magneto-optical (MO) effects refer to various changes in the polarization state of light upon interaction with materials possessing a net magnetic moment, including rotation of the plane of linearly polarized light (Faraday, Kerr rotation), and the complementary differential absorption of left and right circularly polarized light (circular dichroism). In the near visible spectral range these effects result from excitation of electrons in the conduction band. Near x-ray absorption edges, or resonances, magneto-optical effects can be enhanced by transitions from well-defined atomic core levels to transition symmetry selected valence states.

Within the one-particle approximation, the absorption coefficient $\mu_j^\lambda(\omega)$ for incident x-ray polarization λ and photon energy $\hbar\omega$ can be determined as the probability of electronic transitions from initial core states with the total angular momentum j to final unoccupied Bloch states

$$\mu_j^\lambda(\omega) = \sum_{m_j} \sum_{n\mathbf{k}} |\langle \Psi_{n\mathbf{k}} | \Pi_\lambda | \Psi_{jm_j} \rangle|^2 \delta(E_{n\mathbf{k}} - E_{jm_j} - \hbar\omega) \times \theta(E_{n\mathbf{k}} - E_F), \quad (1)$$

where Ψ_{jm_j} and E_{jm_j} are the wave function and the energy of a core state with the projection of the total angular momentum m_j ; $\Psi_{n\mathbf{k}}$ and $E_{n\mathbf{k}}$ are the wave function and the energy of a valence state in the n -th band with the wave vector \mathbf{k} ; E_F is the Fermi energy.

Π_λ is the electron-photon interaction operator in the dipole approximation

$$\Pi_\lambda = -e\boldsymbol{\alpha}\mathbf{a}_\lambda, \quad (2)$$

where $\boldsymbol{\alpha}$ are the Dirac matrices and \mathbf{a}_λ is the λ polarization unit vector of the photon vector potential, with $a_\pm = 1/\sqrt{2}(1, \pm i, 0)$, $a_\parallel = (0, 0, 1)$. Here, $+$ and $-$ denote, respectively, left and right circular photon polarizations with respect to the magnetization direction in the solid. Then, x-ray magnetic circular and linear dichroisms are given by $\mu_+ - \mu_-$ and $\mu_\parallel - (\mu_+ + \mu_-)/2$, respectively. More detailed expressions of the matrix elements in the electric dipole approximation may be found in Refs. [32–34]. The matrix elements due to magnetic dipole and electric quadrupole corrections are presented in Ref. [34].

B. RIXS

Resonant inelastic x-ray scattering refers to the process where the material first absorbs a photon. The system then is excited to a short-lived intermediate state, from which it relaxes radiatively. In an experiment, one studies the x rays emitted in this decay process. The RIXS intensity can in general be presented in terms of a scattering amplitude as [35]

$$I(\omega, \mathbf{k}, \mathbf{k}', \epsilon, \epsilon') = \sum_f |T_{fg}(\mathbf{k}, \mathbf{k}', \epsilon, \epsilon', \omega_{\mathbf{k}})|^2 \times \delta(E_f + \hbar\omega_{\mathbf{k}'} - E_g - \hbar\omega_{\mathbf{k}}), \quad (3)$$

where the delta function enforces energy conservation and the amplitude $T_{fg}(\mathbf{k}, \mathbf{k}', \epsilon, \epsilon', \omega_{\mathbf{k}})$ reflects which excitations are probed and how, for instance, the spectral weights of final state excitations depend on the polarization vectors ϵ and ϵ' of the incoming and outgoing x-rays, respectively.

In the direct RIXS process [35] an incoming photon with energy $\hbar\omega_{\mathbf{k}}$, momentum $\hbar\mathbf{k}$ and polarization ϵ excites the solid from a ground state $|g\rangle$ with energy E_g to the intermediate state $|I\rangle$ with energy E_I . During relaxation the outgoing photon with energy $\hbar\omega_{\mathbf{k}'}$, momentum $\hbar\mathbf{k}'$ and polarization ϵ' is emitted, and the solid is in the state $|f\rangle$ with energy E_f . A valence electron is excited from state \mathbf{k} to states \mathbf{k}' with energy $\hbar\omega = \hbar\omega_{\mathbf{k}} - \hbar\omega_{\mathbf{k}'}$ and momentum transfer $\hbar\mathbf{q} = \hbar\mathbf{k} - \hbar\mathbf{k}'$. Our implementation of the code for the calculation of the RIXS intensity uses Dirac four-component basis functions [36] in the perturbative approach [37]. RIXS is a second-order process, and its intensity is given by

$$I(\omega, \mathbf{k}, \mathbf{k}', \epsilon, \epsilon') \propto \sum_f \left| \sum_I \frac{\langle f | \hat{H}'_{\mathbf{k}'\epsilon'} | I \rangle \langle I | \hat{H}'_{\mathbf{k}\epsilon} | g \rangle}{E_g - E_I} \right|^2 \times \delta(E_f - E_g - \hbar\omega), \quad (4)$$

where the delta function enforces energy conservation, and the photon absorption operator in the dipole approximation is given by the lattice sum $\hat{H}'_{\mathbf{k}\epsilon} = \sum_{\mathbf{R}} \hat{\alpha}\epsilon \exp(-i\mathbf{k}\mathbf{R})$, where $\hat{\alpha}$ are Dirac matrices. Both $|g\rangle$ and $|f\rangle$ states are dispersive so the sum over final states is calculated using the linear tetrahedron method [38]. The matrix elements of the RIXS process in the frame of the fully relativistic Dirac LMTO method were presented in our previous publications [39, 40].

C. Crystal structure

Ta_2NiSe_5 at high temperature possesses an orthorhombic crystal structure (space group $Cmcm$, number 63). The material has a layered structure stacked loosely by a weak van der Waals interaction, and in each layer, Ni single chains and Ta double chains are running along the a

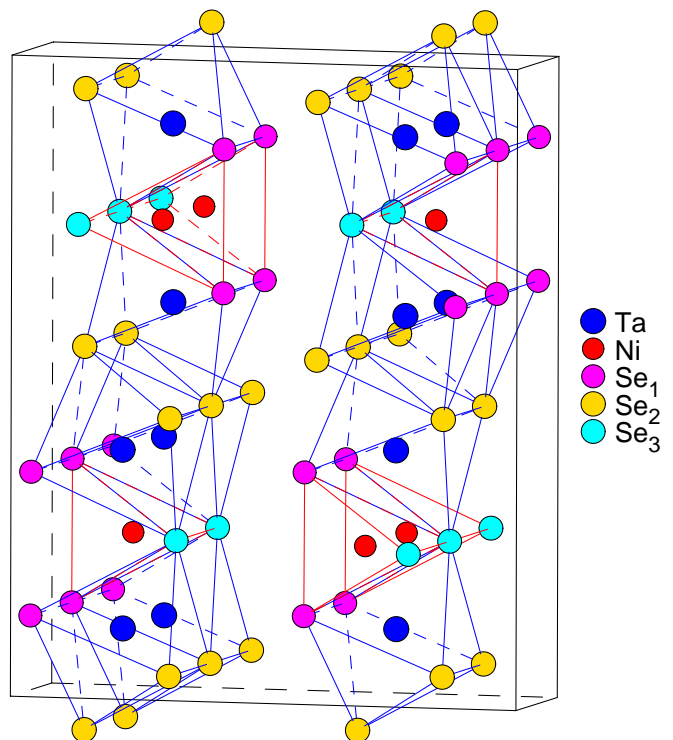


FIG. 1: (Color online) The monoclinic crystal structure of Ta_2NiSe_5 (space group $C12/c1$, number 15) [18]. Blue and red spheres represent Ta and Ni atoms, respectively, magenta, yellow, and green spheres show Se atoms.

axis of the lattice to form a quasi-one-dimensional (1D) chain structure [18]. At critical temperature $T_c = 326$ K, Ta_2NiSe_5 undergoes a second-order transition from an orthorhombic structure to a structure with a subtle monoclinic distortion and reduced electrical conductivity [18, 19].

Figure 1 shows the monoclinic crystal structure of Ta_2NiSe_5 (space group $C12/c1$, number 15) [18]. The Ni and Ta atoms are tetrahedrally and octahedrally coordinated by chalcogen atoms, respectively. The polyhedra are combined by sharing edges to form a repeated unit Ta-Ni-Ta. These chains, which stack in the a direction, are connected via edge-shared octahedra and shared vertices of tetrahedra (Fig. 1). The unit cell contains two such chains displaced by $a/2$ with respect to each other. The coordination about the Ta and Ni atoms is slightly distorted from ideal geometry (Table I).

The primitive unit cell contains four Ta ions, two Ni ions, and ten Se ions. All Ta and Ni sites are crystallographically equivalent but there are three inequivalent Se sites, Se_1 , Se_2 and Se_3 . The Ta-Ta inter-chain distances are fairly large $d_{\text{Ta-Ta}}^\perp = 3.903, 3.980$ Å, so that there is no significant Ta-Ta bonding. Around each Ni atom, however, there are four Ta atoms in a square-planar arrangement with very short Ta-Ni distances $d_{\text{Ta-Ni}} = 2.804, 2.813$ Å. The Ni ions have a tetrahedra NiSe_4 ar-

TABLE I: The atomic positions of Ta_2NiSe_5 . The lattice constants are equal to $a = 3.4974 \text{ \AA}$, $b = 12.8460 \text{ \AA}$ and $c = 15.6457 \text{ \AA}$, $\beta = 90.0^\circ$) for the orthorhombic crystal structure $Cmcm$ [21] and $a = 3.496 \text{ \AA}$, $b = 12.829 \text{ \AA}$ and $c = 15.641 \text{ \AA}$, $\beta = 90.530^\circ$ for the monoclinic structure $C12/c1$ [18].

Structure(Ref.)	Atom	x	y	z
$Cmcm$ [21]	Ta	0.	0.22123	0.11025
	Ni	0.	0.70104	0.25
	Se ₁	0.5	0.08037	0.13776
	Se ₂	0.	0.14583	0.95074
	Se ₃	0.	0.32710	0.25
$C12/c1$ [18]	Ta	-0.00793	0.221349	0.110442
	Ni	0.	0.70113	0.25
	Se ₁	0.50530	0.080385	0.137979
	Se ₂	-0.00513	0.145648	0.950866
	Se ₃	0.	0.32714	0.25

ramentation with $d_{\text{Ni-Se}_1} = 2 \times 2.339 \text{ \AA}$, $d_{\text{Ni-Se}_3} = 2 \times 2.381 \text{ \AA}$. The Ta^{5+} cations are surrounded by Se octahedrons with $d_{\text{Ta-Se}_1} = 2.523, 2.581 \text{ \AA}$, $d_{\text{Ta-Se}_2} = 2.588, 2.661, 2.678 \text{ \AA}$, and $d_{\text{Ta-Se}_3} = 2.570 \text{ \AA}$ interatomic distances. The distance between metals chained along x : $d_{\text{Ta-Ta}}^{\parallel} = d_{\text{Ni-Ni}}^{\parallel} = 2 \times 3.496 \text{ \AA}$ [18].

D. Experimental details

The resonant inelastic x-ray scattering measurement on the Ta L_3 -edge was performed at BL11XU SPring-8. The incident x-ray was monochromatized by a double-crystal Si(111) monochromator and by a secondary 4-bounce Si(333) asymmetric monochromator. π -polarized x-rays with the energy of 9.875 keV were irradiated onto the ac-plane of the Ta_2NiSe_5 crystal, and the horizontally-scattered x-rays were energy-analyzed by a Ge(840) diced analyzer and collected by the Mythen microstrip x-ray detector (Dectris). The total energy resolution was 90 meV. The measurement was performed at a low temperature $\sim 10 \text{ K}$.

E. Calculation details

The details of the computational method are described in our previous papers [40–43] and here we only mention several aspects. The band structure calculations were performed using the fully relativistic LMTO method [33, 44]. This implementation of the LMTO method uses four-component basis functions constructed by solving the Dirac equation inside an atomic sphere [36]. The exchange-correlation functional of the GGA-type was used in the version of Perdew, Burke and Ernzerhof [45]. The Brillouin zone integration was performed using the improved tetrahedron method [46]. The basis consisted of Ta and Ni s , p , d , and f ; and Se s , p , and d LMTO's.

It is widely believed that the $d-d$ excitations show only small momentum transfer vector \mathbf{Q} dependence in $5d$ transition metal compounds [47, 48]. However, the soft RIXS spectra in $3d$ transition metals are more sensitive to the value of \mathbf{Q} . We used in our RIXS calculations $\mathbf{Q} = (0.0625, 1.25, 0)$ at the Ni L_3 and $\mathbf{Q} = (0, 14.5, 0)$ at the Ta L_3 edge, which have been used in the corresponding experimental measurements [31]. We also investigate the dispersion of the RIXS spectra at the Ni and Ta L_3 edges as a function of Q_x .

Note that in our electronic structure calculations, we rely on experimentally measured atomic positions and lattice parameters [18, 21] (see Table I) because they are well established for these materials and are probably still more accurate than those obtained from DFT.

It is known that DFT band calculations usually underestimate the band gap in semiconductors [33]. Because Ta_2NiSe_5 possesses only fully occupied (Ni $3d$ and Se $4p$) and completely empty (Ta $5d$) shells the LDA+ U method is not able to open up a gap [22, 26]. To reproduce a semiconducting ground state in Ta_2NiSe_5 we used a self-interaction-like correction procedure as it was proposed by Kaneko *et al.* [17], where the conduction (valence) bands are shifted upward (downwards) by adding a SIC-like orbital-dependent potential V_i to the Hamiltonian. We used V_i as a parameter and adjusted it to produce the correct value of the band gap and the best agreement with the RIXS experimental spectra.

III. ELECTRONIC STRUCTURE

We found that Ta_2NiSe_5 is a direct-gap semiconductor with the gap minimum at the Γ point of the Brillouin zone in agreement with the experiment [15, 19]. The energy gap for the low temperature $C12/c1$ phase of $\sim 0.16 \text{ eV}$ was estimated from optical measurements [23, 26, 27]. Table II presents the theoretically calculated energy gap ΔE (in eV) for different V_i for the low temperature $C12/c1$ phase.

The shift of Se $4p$ states is the most important in this case. We found that the best agreement for the band gap in this phase can be achieved for $V_{\text{Se}_{4p}} = -5.0 \text{ eV}$ with zero values for the other two parameters (see Table II). It should be mentioned that the self-interaction is the interaction of an electron with its own negative density [29, 30]. Thus, it shifts one electron state to higher energies. Therefore, the use of the negative potential shift for the Se $4p$ and Ni $3d$ states in order to simulate the self-interaction correction is correct. But the addition of a positive potential shift to the Ta $5d$ states cannot be justified in the frame of the SIC method. Moreover, it worsens the agreement of calculated optical spectra [26] as well as the RIXS spectra (see Fig. 7 below) with experimental measurements. It also cannot produce the correct energy band gap (Table II).

Figure 2 presents the energy band structure and total DOS of monoclinic Ta_2NiSe_5 calculated in the fully rela-

TABLE II: The theoretically calculated energy gap ΔE (in eV) for different V_i . The experimental energy gap for the low temperature $C12/c1$ phase was estimated to be ~ 0.16 eV [23, 26, 27].

$V_{Ta_{5d}}$	$V_{Ni_{3d}}$	$V_{Se_{4p}}$	ΔE
0.0	0.0	-2.5	0.0790
0.0	0.0	-4.0	0.1430
0.0	0.0	-5.0	0.1634
0.0	-2.5	-2.5	0.0964
0.0	-4.0	-2.5	0.1123
0.0	-5.0	-2.5	0.1125
0.0	-2.5	-5.0	0.2016
0.0	-4.0	-5.0	0.2282
0.0	-5.0	-5.0	0.2468
2.5	0.0	-2.5	<0
2.5	-2.5	0.0	<0
2.5	-2.5	-2.5	<0
5.0	0.0	-5.0	0.4791
5.0	-5.0	-5.0	0.7907

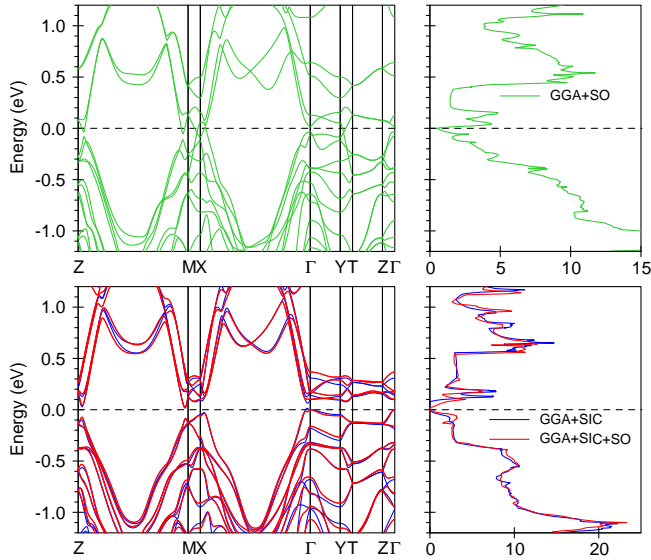


FIG. 2: (Color online) The energy band structure and total density of states (DOS) [in states/(atom eV)] of monoclinic Ta_2NiSe_5 calculated in the fully relativistic Dirac GGA+SO approximation (the upper panel, colors represent the dominant orbital character as marked in the legend) and with taking into account the self-interaction correction (SIC) ($V_{Se_{4p}} = -5.0$ eV) with (red curves) and without (blue curves) SOC (the lower panel).

tivistic Dirac GGA+SO approximation (the top panel) and with taking into account the SIC-like correction ($V_{Se_{4p}} = -5.0$ eV) with (red curves) and without (blue curves) SOC (the lower panel). We found that SOC plays a minor role in the electronic structure and band gap value in Ta_2NiSe_5 .

Figures 3 and 4 show the energy band structure and partial density of states (PDOS) of monoclinic Ta_2NiSe_5

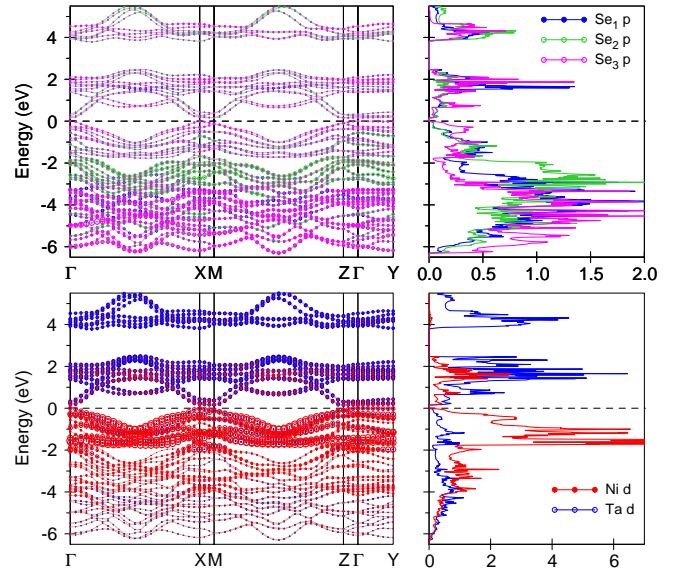


FIG. 3: (Color online) The energy band structure and partial density of states (DOS) of monoclinic Ta_2NiSe_5 calculated in the fully relativistic Dirac GGA+SIC+SO approximation ($V_{Se_{4p}} = -5.0$ eV). Colors represent the dominant orbital character as marked in the legend.

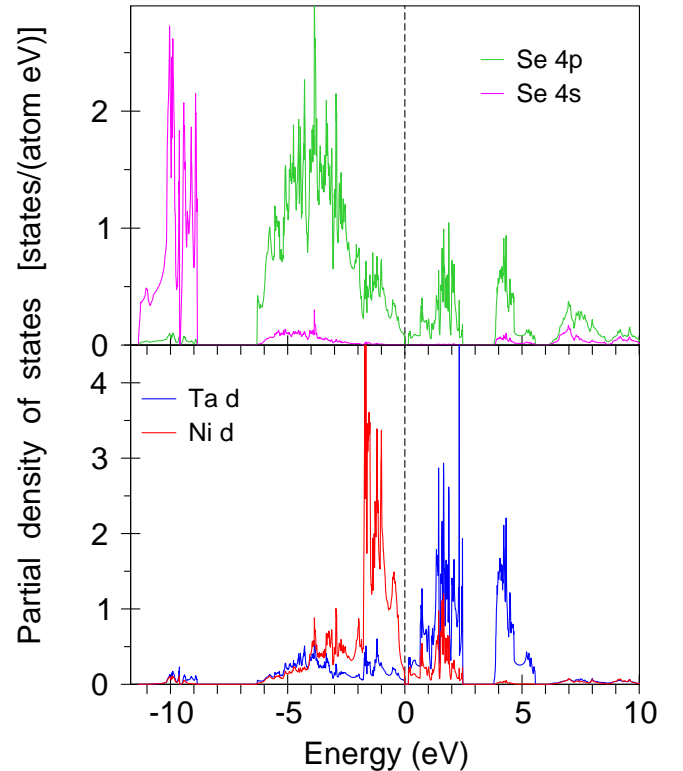


FIG. 4: (Color online) The partial density of states (DOS) of monoclinic Ta_2NiSe_5 calculated in the fully relativistic Dirac GGA+SIC+SO approximation ($V_{Se_{4p}} = -5.0$ eV).

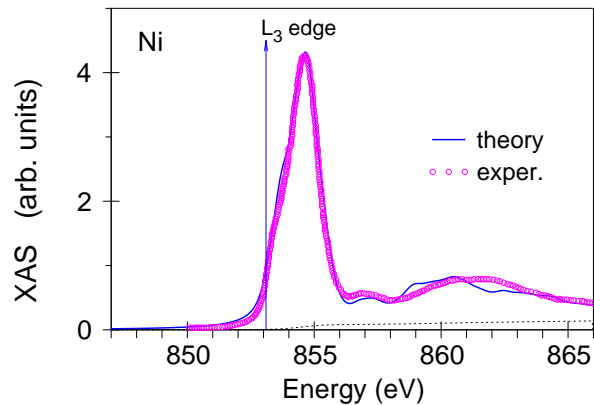


FIG. 5: (Color online) The theoretically calculated (the full blue curve) and experimentally measured [31] (open magenta circles) x-ray absorption spectroscopy (XAS) spectra at the Ni L_3 edge.

calculated in the fully relativistic Dirac GGA+SIC+SO approximation ($V_{Se4p} = -5.0$ eV). Se $4s$ states are located from -11.4 to -8.85 eV, Se $4p$ states occupy a rather large energy interval from -6.3 to 2.5 eV and between 3.8 and 10 eV. They are strongly hybridize with the Ni $3d$ valent states and Ta $5d$ conduction states. The fully occupied Ni $3d$ states are situated between -1.9 eV and E_F . There are some Ni $3d$ states at the bottom of the valent band between -6.3 and -1.9 eV, which occur from the strong hybridization with Se $4p$ states. Ta t_{2g} states are situated between 0.16 and 2.5 eV. Ta e_g states are separated from the Ta t_{2g} states by a band gap of 1.3 eV and occupy the energy interval from 3.8 to 5.6 eV. Although formally the Ta valency in Ta_2NiSe_5 is close to Ta^{5+} ($5d^0$) the occupation number of $5d$ electrons in the Ta atomic sphere is equal to 2.6 . The excessive charge is provided by the tails of Se $4p$ and Ni $3d$ states. These $5d_{Se}$ and $5d_{Ni}$ states play an essential role in the RIXS spectrum at the Ta L_3 edge (see Section V).

IV. X-RAY ABSORPTION SPECTRA

Figures 5 and 6 show the theoretically calculated (full blue curves) XAS spectra compared with the experimentally measured spectra at the Ni L_3 [31] and Ta L_3 [27] edges, respectively. Although Ni L_3 XAS extends more than 15 eV above the edge, the major peak situated at 1.5 eV above the edge is very narrow with a half-width of ~ 2 eV. The peak possesses a low energy shoulder at 0.6 eV above the edge. The spectrum reflects the energy distribution of the Ni $3d$ states which are located between 0.16 and 2.5 eV (see Fig. 4). The major peak is created by the states situated between 1.2 and 2.5 eV, and the low energy shoulder is due to the states at 0.16 – 1.0 eV. Ni $3d$ PDOS is very small above 3.5 eV (see Fig. 4), which leads to relatively small fine structures in Ni L_3 XAS

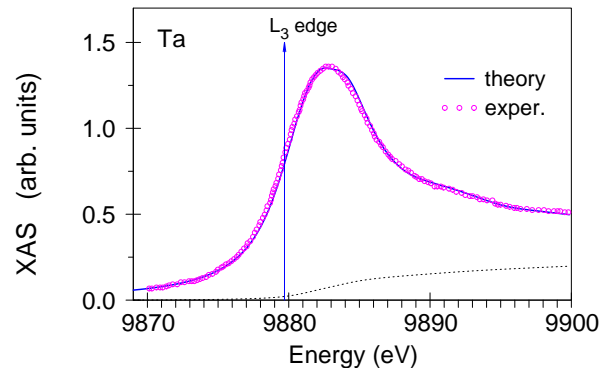


FIG. 6: (Color online) The theoretically calculated (the full blue curve) and experimentally measured [27] (open magenta circles) x-ray absorption spectroscopy (XAS) spectra at the Ta L_3 edge.

above 856 eV. The peak at 857 eV is due to transitions into the Ni $3d$ empty states which are derived from the hybridization with Ta $5d$ states while the fine structures between 859 and 866 eV are due to the hybridization with free electron-like states.

Ta L_3 XAS has an almost four times larger half-width (Fig. 6) in comparison with Ni L_3 XAS because it reflects the energy distribution of the Ta t_{2g} and e_g states situated at 0.16 – 2.5 eV and 3.8 – 5.6 eV, respectively. Besides, the width of the Ta $3p_{3/2}$ core level is much larger than that of Ni $3p_{3/2}$ (4.68 and 0.47 eV, respectively [49]). The band structure calculations reproduce well the XAS spectra at the Ni and Ta L_3 edges.

V. RIXS SPECTRA

A. Ni L_3 RIXS spectrum

The experimental RIXS spectrum at the Ni L_3 edge in Ta_2NiSe_5 was measured by Monney *et al.* [31] and Lu *et al.* [27] in the energy interval up to 6 and 1.2 eV, respectively. The RIXS spectrum occupies a relatively small energy interval and possesses several fine structures.

Figure 7 presents the influence of the SIC parameter V_i on the shape of the Ni L_3 RIXS spectrum. We obtained reasonably good agreement with the experiment applying V_i only to the Se $4p$ states. Using $V_{Se4p} = -2.5$ eV, we describe better the low-energy part of the spectrum, while its high-energy part is described better by $V_{Se4p} = -5.0$ eV. Applying the SIC parameter to Ni $3d$ and/or Ta $5d$ states makes the agreement with the experiment only worsen.

Figure 8 shows the Ni L_3 RIXS spectrum as a function of incident photon energy above the corresponding edge. We found that the fine structure between 3 and 4 eV is increased with increasing the incident photon energy. It is in qualitative agreement with the corresponding ex-

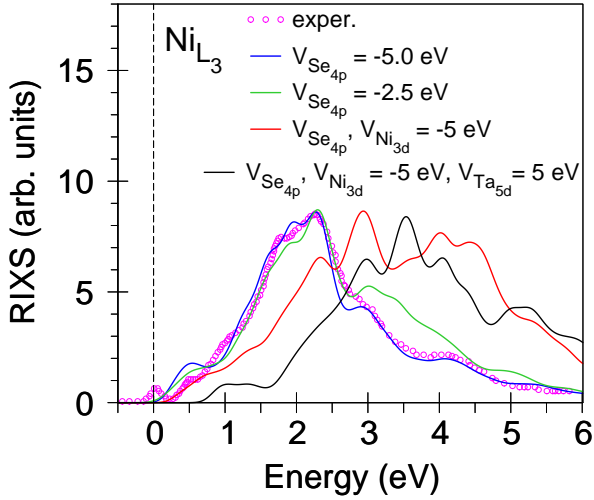


FIG. 7: (Color online) The experimental resonant inelastic x-ray scattering (RIXS) spectrum at the Ni L_3 edge [31] in near-specular geometry $\mathbf{Q} = (0.0625, 1.25, 0)$ in reciprocal lattice units for incident photon energy $\hbar\omega_{in} = 853.3$ eV compared with the theoretical RIXS spectra for the same geometry and the incident photon energy calculated in the GGA+SIC+SO approximation for different parameters V_i .

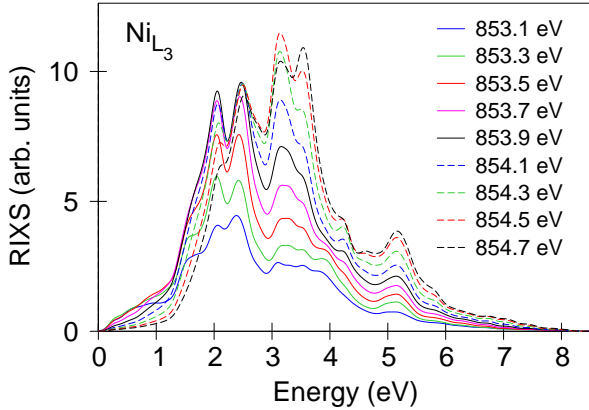


FIG. 8: (Color online) Resonant inelastic x-ray scattering (RIXS) spectra as a function of incident photon energy, calculated at the Ni L_3 edge with momentum transfer vector $\mathbf{Q} = (0.0625, 1.25, 0)$ in reciprocal lattice units.

perimental dependence, however, the experiment shows weaker dependence [31].

It is widely believed that the $d-d$ excitations show only small momentum transfer vector \mathbf{Q} dependence in $5d$ transition metal compounds [47, 48]. However, the soft RIXS spectra in $3d$ transition metals are more sensitive to the value of \mathbf{Q} . Figure 9 shows RIXS spectra at the Ni L_3 edge calculated as a function of Q_x in $\mathbf{Q} = (Q_x, 1.25, 0)$ for incident photon energy $\hbar\omega_{in} = 853.3$ eV. We found that with the increasing of Q_x the low-energy peak at 1 eV is significantly increased. The fine structure at

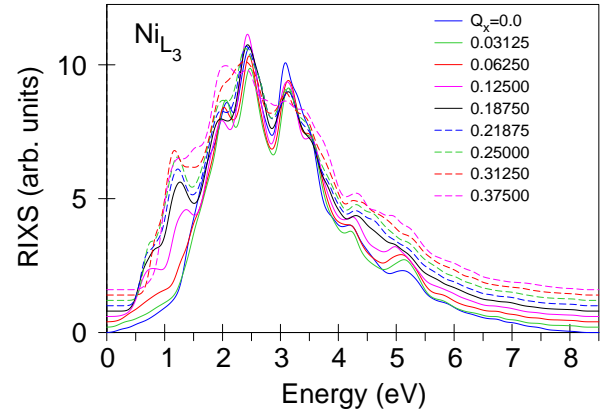


FIG. 9: (Color online) Resonant inelastic x-ray scattering (RIXS) spectra at the Ni L_3 edge calculated as a function of Q_x in the momentum transfer vector $\mathbf{Q} = (Q_x, 1.25, 0)$ for incident photon energy $\hbar\omega_{in} = 853.3$ eV.

2 eV is also increased but to a lesser extent. The similar dependence was also observed experimentally, however, it is weaker in the experiment [31].

The experimentally measured RIXS spectrum consists of a peak centered at zero energy loss, which comprises the elastic line and other low-energy features such as phonons, magnons, etc., and at least six inelastic excitations. Figure 10 (the lower panel) presents the experimental RIXS spectrum at the Ni L_3 edge [31] (open magenta circles) for $\mathbf{Q} = (0.0625, 1.25, 0)$ in reciprocal lattice units and incident photon energy $\hbar\omega_{in} = 853.3$ eV compared with the theoretical RIXS spectrum calculated for the same geometry in the GGA+SIC+SO approximation with $V_{Se4p} = -5.0$ eV (the full blue curve) and partial contributions from different interband transitions presented in Fig. 11 by different colors. We can divide the Ni $3d$ valence band in Fig. 11 into two groups. The bands number 1 situated between -6.3 and -1.8 eV are the Ni $3d_{Se}$ states which are derived from the decomposition of Se $4p$ states inside the Ni atomic spheres. The bands situated between -1.8 eV and E_F are Ni $3d$ states themselves. We divide the latter bands into three groups with numbers from 2 to 4. The empty Ni $3d$ bands we subdivide into two groups with numbers 5 and 6. We found that the first four fine structures (*a*, *b*, *c*, and *d*) of the Ni L_3 RIXS spectrum are derived from interband transitions from the occupied bands with numbers 2 to 4 to the empty bands number 5. The low-energy peak *a* is due to interband transition between the closest to the Fermi level bands 4 and 5. The same transitions also contribute to the low-energy shoulder *c*. The major peak *d* is derived from $3 \rightarrow 5$ and $4 \rightarrow 5$ transitions. The high-energy fine structure *d* is due to interband transitions from all occupied bands (besides bands 1) to the group of empty bands by number 6. The highest energy structure *f* is due to transitions from the Ni $3d_{Se}$ states (bands 1) to empty states with numbers 5 and 6. It

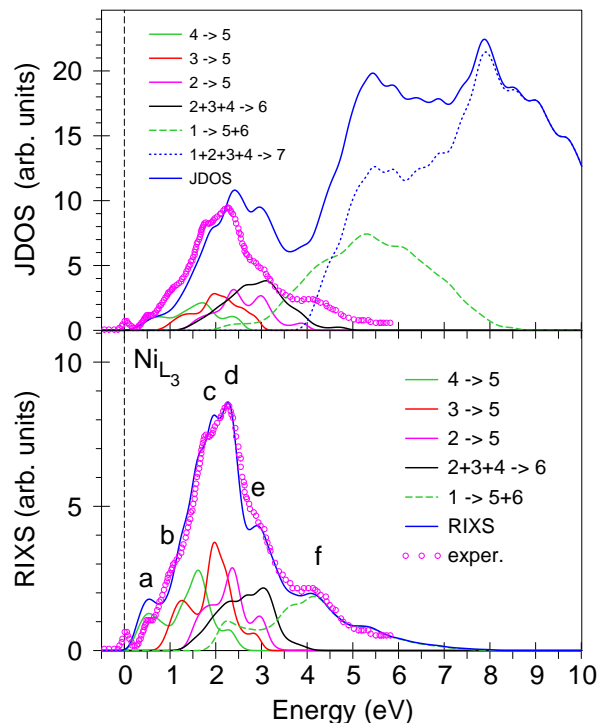


FIG. 10: (Color online) The lower panel: the experimentally measured resonant inelastic x-ray scattering (RIXS) spectrum at the Ni L_3 edge [31] (open magenta circles) in near-specular geometry $\mathbf{Q} = (0.0625, 1.25, 0)$ for incident photon energy $\hbar\omega_{in} = 853.3$ eV compared with the theoretical RIXS spectra calculated for the same geometry and incident photon energy in the GGA+SIC+SO approximation with $V_{Se_{4p}} = -5.0$ eV (the full blue curve) and partial contributions from different interband transitions presented in Fig. 11. The upper panel: joint density of states (JDOS) (the full blue curve) and partial transitions from different interband transitions in comparison with the experimental RIXS spectrum (open magenta circles).

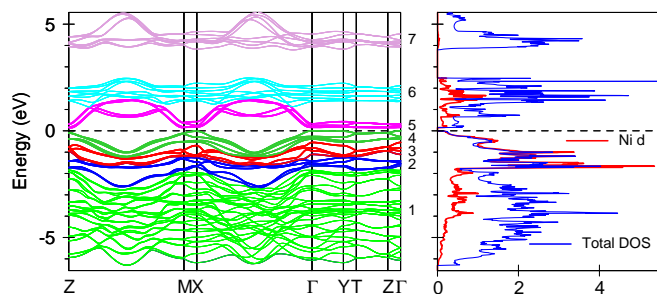


FIG. 11: (Color online) The energy band structure, partial Ni 3d density of states (DOS) [in states/(atom eV)] (the red curve) and normalized total DOS (the blue curve) of monoclinic Ta₂NiSe₅ calculated in the fully relativistic Dirac GGA+SIC+SO approximation ($V_{Se_{4p}} = -5.0$ eV).

is important to note that all these interband transitions strongly overlap with each other.

Analyzing different interband transitions we found

that $(2+3+4) \rightarrow 5$ transitions are larger than $(2+3+4) \rightarrow 6$ transitions. RIXS is an element- and orbital-selective X-ray spectroscopy technique, based on a two-step, two-photon resonant process. It combines X-ray emission spectroscopy (XES) with X-ray absorption spectroscopy by measuring the coherent X-ray emission at an incident X-ray photon energy within the near edge X-ray absorption spectrum. In the first step (X-ray absorption) in our case, an electron of the absorbing atom is resonantly excited from a $2p_{3/2}$ core level into a 5 or 6 empty energy bands. In the second step (X-ray emission), the system radiatively decays from the $(2+3+4)$ occupied bands into the $2p_{3/2}$ core level, accompanied by a photon-out emission. Because the X-ray emission is the same for both the cases, we have consider only absorption process into bands 5 and 6 separately. Ref. [43] presents the angular matrix elements for dipole allowed transitions at the L_3 edge from initial core states with different projections m_j of the total angular momentum $j = 3/2$ to d cubic harmonics. It was shown that for the σ incident light the largest contribution is due to $2p_{3/2} \rightarrow d_{xy}$ and $2p_{3/2} \rightarrow d_{x^2-y^2}$ transitions (two times larger than the transitions into d_{yz} and d_{xz} states and three times larger than the transitions into d_{3z^2-1} states). Figure 12 presents orbital resolved Ni 3d DOS. The bands number 5 are derived mostly from d_{xy} orbitals, bands 6 are from d_{xz} , d_{yz} , and d_{3z^2-1} orbitals. It explains why the $(2+3+4) \rightarrow 5$ transitions exceed the $(2+3+4) \rightarrow 6$ ones.

The upper panel of Fig. 10 shows JDOS (the full blue curve) and partial transitions from different interband transitions in comparison with the experimental RIXS spectrum. JDOS is not able to describe correctly the the RIXS spectrum above 2 eV. It can be explained by the difference in the shape of the total and partial Ni 3d DOS presented in Fig. 11 (blue and red curves on the right panel, respectively). We normalized total DOS to Ni PDOS at -1.6 eV. Total DOS of the band group number 1 is significantly larger in comparison with Ni PDOS at the same energy interval. As a result, the intensity of $1 \rightarrow (5+6)$ transitions is significantly increased for JDOS. Besides, new very intensive transitions $(1+2+3+4) \rightarrow 7$ appear, which are completely absent in the theoretically calculated RIXS spectrum. The RIXS spectrum at the Ni L_3 edge can be correctly described only with taking into account corresponding matrix elements.

B. Ta L_3 RIXS spectrum

Figure 13 presents the influence of the SIC parameter V_i on the shape of the Ta L_3 RIXS spectrum. This parameter is less critical than in the Ni L_3 RIXS spectrum. The combination of the parameters $(V_{Ta_{5d}}, V_{Ni_{3d}}, V_{Se_{4p}}) = (0, -5, -5)$, $(0, 0, -5)$, and $(0, 0, -2.5)$ eV give similar Ta L_3 RIXS spectra, although, the last combination produces a slightly better description of the low-energy shoulder at ~ 2.5 eV. Applying an additional SIC parameter V_i to the Ta 5d states makes the agreement with the

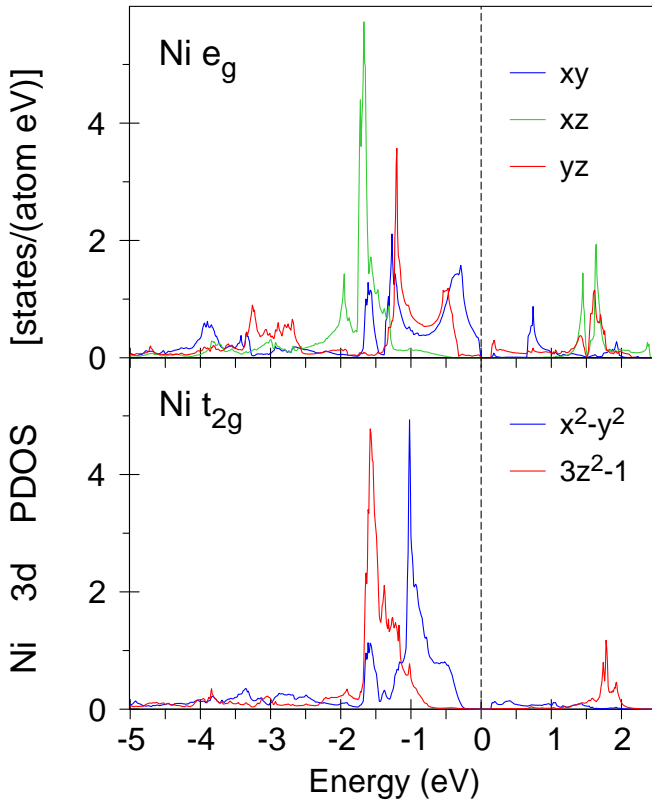


FIG. 12: (Color online) Orbital resolved Ni 3d density of states (DOS) [in states/(atom eV)] of monoclinic Ta_2NiSe_5 calculated in the fully relativistic Dirac GGA+SIC+SO approximation ($V_{\text{Se}_{4p}} = -5.0$ eV).

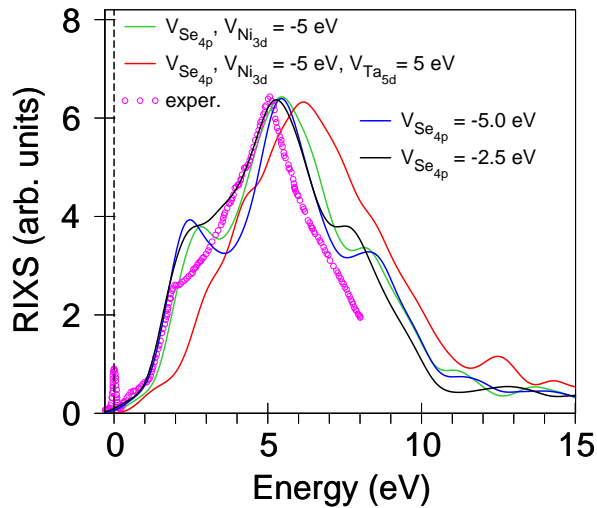


FIG. 13: (Color online) The experimental resonant inelastic x-ray scattering (RIXS) spectrum at the Ta L_3 edge compared with the theoretical RIXS spectra calculated in the GGA+SIC+SO approximation for different parameters V_i .

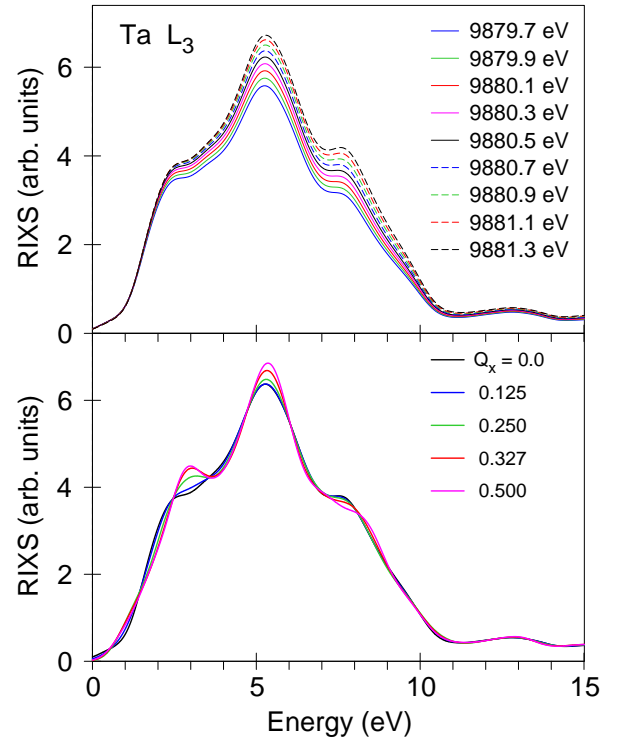


FIG. 14: (Color online) The lower panel: resonant inelastic x-ray scattering (RIXS) spectra at the Ta L_3 edge calculated as a function of Q_x in the momentum transfer vector $\mathbf{Q} = (Q_x, 14.5, 0)$ for incident photon energy $\hbar\omega_{in} = 9679.7$ eV. The upper panel: RIXS spectra as a function of incident photon energy calculated at the Ta L_3 edge with $\mathbf{Q} = (0, 14.5, 0)$ in reciprocal lattice units.

experiment worse.

Figure 14 shows the theoretically calculated RIXS spectra at the Ta L_3 edge as a function of incident photon energy (the upper panel), and as a function of Q_x in the momentum transfer vector $\mathbf{Q} = (Q_x, 14.5, 0)$ (the lower panel). RIXS spectrum at the Ta L_3 edge possesses relatively weak dependence from incident photon energy as well as from the momentum transfer vector \mathbf{Q} in comparison with the corresponding dependences at the Ni L_3 edge (compare Fig. 14 with Figs. 8 and 9). It is in agreement with the Krajewska *et al.* who claimed that the $d-d$ excitations show only a small momentum transfer vector \mathbf{Q} dependence in the $5d$ transition metal compounds [48].

Figure 15 presents the experimental RIXS spectrum at the Ta L_3 edge compared with the theoretically calculated one (the full black curve) and partial contributions from different interband transitions. Because the Ta valency in Ta_2NiSe_5 is close to Ta^{5+} ($5d^0$) the Ta L_3 RIXS spectrum is formed by a charge transfer between occupied $5d_{Se}$ and $5d_{Ni}$ states (see Fig. 4) and empty t_{2g} and e_g states (blue and red curves in Fig. 15, respectively). The transitions into the other empty states are very small (the green curve in Fig. 15). Empty total

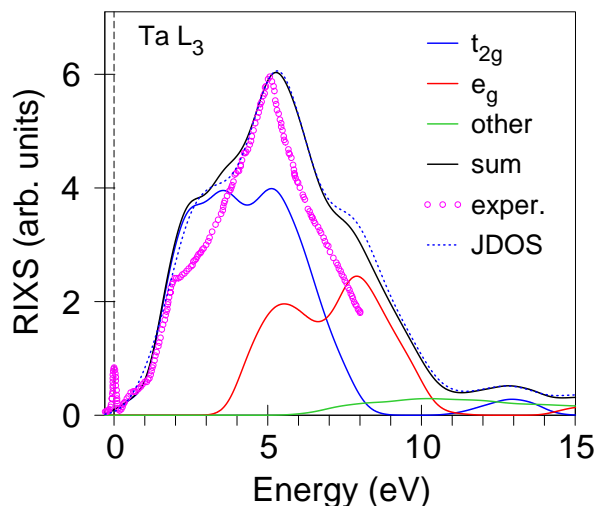


FIG. 15: (Color online) The experimental resonant inelastic x-ray scattering (RIXS) spectrum at the Ta L_3 edge (open magenta circles) compared with the theoretically calculated one (the full black curve) and partial contributions from different interband transitions for the momentum transfer vector $\mathbf{Q} = (0, 14.5, 0)$ in reciprocal lattice units. The dotted blue curve presents joint density of states (JDOS).

DOS in Ta_2NiSe_5 is formed mostly by Ta $5d$ states, besides, the energy distribution of the occupied part of Ta $5d$ PDOS, which is formed by the tails of Se $4p$ and Ni $3d$ states inside the Ta atomic spheres, repeats the shape of total DOS, therefore, JDOS describes quite well the RIXS spectrum at the Ta L_3 edge (the dotted blue curve in Fig. 15).

VI. CONCLUSIONS

The electronic and magnetic properties of quasi-one-dimensional Ta_2NiSe_5 were investigated theoretically in the frame of the fully relativistic spin-polarized Dirac LMTO band-structure method. We found that SOC plays a minor role in the electronic structure of Ta_2NiSe_5 . The GGA approximation produces a metallic ground state in Ta_2NiSe_5 in contradiction with ARPES, dc transport, and optical measurements, which indicate that Ta_2NiSe_5 is a small band-gap semiconductor. To obtain the semiconducting ground state in Ta_2NiSe_5 we use a SIC-like orbital-dependent potential V_l incorporated into the Hamiltonian. Although the correct value of the band gap can be achieved using different combinations of the parameters $V_{\text{Ta}5d}$, $V_{\text{Ni}3d}$, and $V_{\text{Se}4p}$, the shift of Se $4p$ states is most important in Ta_2NiSe_5 . To reproduce the experimental energy gap and get the best agreement be-

tween the theory and different experiments we applied the orbital-dependent potential V_l for the Se $4p$ states only. We found that the value of $V_{\text{Se}4p}$ is somewhere between -2.5 and -5.0 eV. The value $V_{\text{Se}4p} = -2.5$ eV describes better the low-energy parts of Ni and Ta L_3 RIXS spectra, while the value -5.0 eV describes better the high-energy part of the Ni RIXS spectrum and produces the correct value of the energy band gap.

We investigated experimentally the RIXS spectrum at the Ta L_3 edge and theoretically at the Ni and Ta L_3 edges in Ta_2NiSe_5 . The experimentally measured RIXS spectrum at the Ni L_3 edge in addition to the elastic scattering peak at 0 eV possesses several features. We interpret these structures by analyzing particular interband transitions. We investigated the RIXS spectra at the Ni and Ta L_3 edges as a function of momentum transfer vector \mathbf{Q} and incident photon energy. The RIXS spectrum at the Ta L_3 edge possesses relatively weak dependence on the incident photon energy as well as on the \mathbf{Q} vector. The RIXS spectrum at the Ni L_3 edge shows a strong increase of the low-energy peak at ~ 1 eV with an increase of the Q_x component of the vector \mathbf{Q} . The increase of the incident photon energy $\hbar\omega_{in}$ above the Ni L_3 edge leads to an increase of the RIXS spectrum in the energy range from 3 to 4 eV.

Because Ta_2NiSe_5 possesses only fully occupied and completely empty shells with the formal valencies Ta^{5+} ($5d^0$), Ni^0 ($3d^{10}$), and Se^{2-} ($4p^6$), both the Ni and Ta L_3 RIXS spectra belong to a charge transfer type with ligand-to-metal transitions. In the case of Ni L_3 RIXS, these transitions are between occupied Ni $3d$ and empty Ni $3d_{\text{Ta}}$ states derived from the tails of Ta $5d$ states inside the Ni atomic spheres. The Ta L_3 RIXS spectrum is formed by interband transitions to empty Ta $5d$ states from occupied $5d_{\text{Se}}$ and $5d_{\text{Ni}}$ states derived from the tails of Se $4p$ and Ni $3d$ states.

Empty total DOS in Ta_2NiSe_5 is formed mostly by Ta $5d$ states and the energy distribution of the occupied part of Ta $5d$ PDOS, which is formed by the tails of the Se $4p$ and Ni $3d$ states inside the Ta atomic spheres, repeats the shape of total DOS, therefore, JDOS describes quite well the RIXS spectrum at the Ta L_3 edge. However, the Ni L_3 RIXS spectrum can be correctly described only with taking into account corresponding matrix elements.

Acknowledgments

RIXS experiments at the Ta L_3 -edge were performed at the BL11XU of SPring-8 with the approval of the Japan Synchrotron Radiation Research Institute (JASRI) (Proposals No. 2016A3552 and No. 2016BA3552).

[1] W. Witczak-Krempa, G. Chen, Y. B. Kim, and L. Balents, *Annu. Rev. Condens. Matter Phys.* **5**, 57 (2014).

[2] X.-L. Qi and S.-C. Zhang, *Physics Today* **63**, 33 (2010).

- [3] Y. Ando, J. Phys. Soc. Jpn. **82**, 102001 (2013).
- [4] T. O. Wehling, A. Black-Schafferc, and A. Balatsky, Adv. Phys. **63**, 1 (2014).
- [5] A. Bansil, L. H. and T. Das, Rev. Mod. Phys. **88**, 021004 (2016).
- [6] B. J. Kim, H. Jin, S. J. Moon, J.-Y. Kim, B.-G. Park, C. S. Leem, J. Yu, T. W. Noh, C. Kim, S.-J. Oh, et al., Phys. Rev. Lett. **101**, 076402 (2008).
- [7] B. J. Kim, H. Ohsumi, T. Komesu, S. Sakai, T. Morita, H. Takagi, and T. Arima, Science **323**, 1329 (2009).
- [8] G. Jackeli and G. Khaliullin, Phys. Rev. Lett. **102**, 017205 (2009).
- [9] H. Watanabe, T. Shirakawa, and S. Yunoki, Phys. Rev. Lett. **105**, 216410 (2010).
- [10] C. Martins, M. Aichhorn, L. Vaugier, and S. Biermann, Phys. Rev. Lett. **107**, 266404 (2011).
- [11] W. Witczak-Krempa and Y. B. Kim, Phys. Rev. B **85**, 045124 (2012).
- [12] A. Go, W. Witczak-Krempa, G. S. Jeon, K. Park, and Y. B. Kim, Phys. Rev. Lett. **109**, 066401 (2012).
- [13] A. B. Sushkov, J. B. Hofmann, G. S. Jenkins, J. Ishikawa, S. Nakatsuji, S. DasSarma, and H. D. Drew, Phys. Rev. B **92**, 241108 (2015).
- [14] I. Kimchi, J. G. Analytis, and A. Vishwanath, Phys. Rev. B **90**, 205126 (2014).
- [15] Y. Wakisaka, T. Sudayama, K. Takubo, T. Mizokawa, M. Arita, H. Namatame, M. Taniguchi, N. Katayama, M. Nohara, and H. Takagi, Phys. Rev. Lett. **103**, 026402 (2009).
- [16] Y. Wakisaka, T. Sudayama, K. Takubo, T. Mizokawa, N. L. Saini, M. Arita, H. Namatame, M. Taniguchi, N. Katayama, M. Nohara, et al., J. Supercond. Nov. Magn. **25**, 1231 (2012).
- [17] T. Kaneko, T. Toriyama, T. Konishi, and Y. Ohta, Phys. Rev. B **87**, 035121 (2013).
- [18] S. A. Sunshine and J. A. Ibers, Inorg. Chem. **24**, 3611 (1985).
- [19] F. J. DiSalvo, C. H. Chen, R. M. Fleming, J. V. Waszczak, R. G. Dunn, S. A. Sunshine, and J. A. Ibers, J. Less-Common Met. **27**, 116 (1986).
- [20] K. Fukutani, R. Stania, J. Jung, E. F. Schwier, K. Shimada, C. I. Kwon, J. S. Kim, and H. W. Yeom, Phys. Rev. Lett. **123**, 206401 (2019).
- [21] M. D. Watson, I. Markovi, E. A. Morales, P. L. Fevre, M. Merz, A. A. Haghighirad, and P. D. C. King, Phys. Rev. Res. **2**, 013236 (2020).
- [22] J. Lee, C.-J. Kang, M. J. Eom, J. S. Kim, B. I. Min, and H. W. Yeom, Phys. Rev. B **99**, 075408 (2019).
- [23] Y. F. Lu, H. Kono, T. I. Larkin, A. W. Rost, T. Takayama, A. V. Boris, B. Keimer, and H. Takagi, Nat. Commun. **8**, 14408 (2017).
- [24] K. Seki, Y. Wakisaka, T. Kaneko, T. Toriyama, T. Konishi, T. Sudayama, N. L. Saini, M. Arita, H. Namatame, M. Taniguchi, et al., Phys. Rev. B **90**, 155116 (2014).
- [25] S. Mor, M. Herzog, D. Golez, P. Werner, M. Eckstein, N. Katayama, M. Nohara, H. Takagi, T. Mizokawa, C. Monney, et al., Phys. Rev. Lett. **119**, 086401 (2017).
- [26] T. I. Larkin, A. N. Yaresko, D. Pröpper, K. A. Kikoin, Y. F. Lu, T. Takayama, Y.-L. Mathis, A. W. Rost, H. Takagi, B. Keimer, et al., Phys. Rev. B **95**, 195144 (2017).
- [27] H. Lu, M. Rossi, J. Kim, H. Yavas, A. Said, A. Nag, M. Garcia-Fernandez, S. Agrestini, K.-J. Zhou, C. Jia, et al., Phys. Rev. B **103**, 235159 (2021).
- [28] D. Werdehausen, T. Takayama, M. Höppner, G. Albrecht, A. W. Rost, Y. Lu, D. Manske, H. Takagi, and S. Kaiser, Science Advances **4**, 3 (2018).
- [29] J. P. Perdew and A. Zunger, Phys. Rev. B **23**, 5048 (1981).
- [30] H. Lin, R. S. Markiewicz, L. A. Wray, L. Fu, M. Z. Hasan, and A. Bansil, Phys. Rev. Lett. **105**, 036404 (2010).
- [31] C. Monney, M. Herzog, A. Pulkkinen, Y. Huang, J. Pellicciari, P. Olalde-Velasco, N. Katayama, M. Nohara, H. Takagi, T. Schmitt, et al., Phys. Rev. B **102**, 085148 (2020).
- [32] G. Y. Guo, H. Ebert, W. M. Temmerman, and P. J. Durham, Phys. Rev. B **50**, 3861 (1994).
- [33] V. Antonov, B. Harmon, and A. Yaresko, *Electronic Structure and Magneto-Optical Properties of Solids* (Kluwer, Dordrecht, 2004).
- [34] E. Arola, M. Horne, P. Strange, H. Winter, Z. Szotek, and W. M. Temmerman, Phys. Rev. B **70**, 235127 (2004).
- [35] L. J. P. Ament, M. van Veenendaal, T. P. Devereaux, J. P. Hill, and J. van den Brink, Rev. Mod. Phys. **83**, 705 (2011).
- [36] V. V. Nemoshkalenko, A. E. Krasovskii, V. N. Antonov, V. N. Antonov, U. Fleck, H. Wonn, and P. Ziesche, Phys. status solidi B **120**, 283 (1983).
- [37] E. Arola, P. Strange, and B. L. Gyorffy, Phys. Rev. B **55**, 472 (1997).
- [38] G. Lehmann and M. Taut, Phys. status solidi B **54**, 469 (1972).
- [39] D. A. Kukusta and A. N. Yaresko, in *Band structure approach to RIXS* (EBS workshop on X-ray Spectroscopy of Magnetic Materials. ESRF, Grenoble, 7–9 October 2019, unpublished).
- [40] V. N. Antonov, D. A. Kukusta, and L. V. Bekenov, Phys. Rev. B **105**, 155144 (2022).
- [41] V. N. Antonov, O. Jepsen, A. N. Yaresko, and A. P. Shpak, J. Appl. Phys. **100**, 043711 (2006).
- [42] V. N. Antonov, B. N. Harmon, A. N. Yaresko, and A. P. Shpak, Phys. Rev. B **75**, 184422 (2007).
- [43] V. N. Antonov, A. N. Yaresko, and O. Jepsen, Phys. Rev. B **81**, 075209 (2010).
- [44] O. K. Andersen, Phys. Rev. B **12**, 3060 (1975).
- [45] J. P. Perdew, K. Burke, and M. Ernzerhof, Phys. Rev. Lett. **77**, 3865 (1996).
- [46] P. E. Blöchl, O. Jepsen, and O. K. Andersen, Phys. Rev. B **49**, 16223 (1994).
- [47] X. Liu, V. M. Katukuri, L. Hozoi, W.-G. Yin, M. P. M. Dean, M. H. Upton, J. Kim, D. Casa, A. Said, T. Gog, et al., Phys. Rev. Lett. **109**, 157401 (2012).
- [48] A. Krajewska, T. Takayama, R. Dinnebier, A. Yaresko, K. Ishii, M. Isobe, and H. Takagi, Phys. Rev. B **101**, 121101(R) (2020).
- [49] J. L. Campbell and T. Parr, At. Data Nucl. Data Tables **77**, 1 (2001).